Available online at www.sciencedirect.com

ScienceDirect

INDAER

Journal of Wind Engineering & Industrial Aerodynamics 00 (2015) 1–17

A Computational Assessment of the Aerodynamic Performance of a Tilted Darrieus Wind Turbine

Gabriele Bedon*, Stefano De Betta, Ernesto Benini

Department of Industrial Engineering, University of Padua, Via Venezia 1, 35131 Padua, Italy

Abstract

The aerodynamic performance of a Darrieus wind turbine operating with the rotation axis tilted with respect to the free-stream wind speed is investigated in this paper. An Unsteady Reynolds Averaged Navier Stokes (URANS) Computational Fluid Dynamics (CFD) model is proposed in order to provide wind turbine manufacturers with a reliable simulation tool to forecast the power conversion characteristics of vertical axis wind turbine prototypes that operate in tilted conditions. The outputs of the model are compared against experimental performance of a non-tilted rotor corrected to the standard sea level conditions. Two different tilted configurations are studied (i.e., a tilt angle of 10° and 20°), and the aerodynamic performance are presented in terms of the mechanical power production and the power coefficient. A sensible decrease in the power production is observed for increasing tilt angles. Comprehensive physical interpretations of the results are provided, considering also the predictions of a methodology based on semi-empirical methods.

Keywords: Vertical Axis Wind Turbines, Tilted Darrieus, 3D URANS CFD, Offshore Wind Turbines

1. Introduction

During the last decade, wind energy has experienced a cubic growth [1] due to the increasing awareness for the need of a renewable energy source that could provide humanity with a solution to overcome the actual fossil fuel dependency. In this regard, the ongoing research on wind turbine technology development has resulted in new concepts that improve the production and reduce the cost of energy.

Similarly to horizontal axis wind turbines, which are now being constructed in offshore locations in order to exploit the observed higher power density and increase its size without incurring Not In My Back Yard (NIMBY) issues, Vertical Axis Wind Turbines (VAWTs) are also recently object of research activities in order to prove the feasibility of offshore configurations with sensibly increased size. Among the different VAWTs types, Darrieus wind turbines are the most interesting due to the higher efficiencies and reduced loads compared to other configurations.

*Corresponding author, email: gabriele.bedon@dii.unipd.it, tel. +39 049 8276770

Experimental tests on Darrieus turbines with increasing size were performed in the recent past by the most important research centers. Literature provides the aerodynamic performance for rotors with characteristic lengths of 2 meters [2], 5 meters [3], 17 meters [4, 5], 34 meters [6], 37 meters [7, 8], and 96 meters [9, 10]. These tests provided the most reliable experimental results for the performance of these machines and enable wind turbine designers to perform validation studies of their simulation methods over the widest range of Darrieus configurations [11].

Based on the experience of onshore installations, a variety of research projects aimed to deploy Darrieus wind turbines in offshore environments. Differently from horizontal axis wind turbines, whose installations generally include foundation technologies that constraint the turbine movement (e.g., monopile, gravity base, tripod base, and jacket structures) [12, 13, 14], a floating concept is being analysed for vertical axis wind turbines, which would allow its installation in deeper waters [15].

Nowadays two main projects are being conducted by the main institutions of the offshore vertical axis wind turbine research. The *Inflow* project [16] aims at demonstrating the cost competitiveness and provide an industrial prototype of a helical Darrieus turbine that might be installed on a semi-submersible floater support structure. A 26 MW wind farm is designed as target to complete the first phase of its industrialization process, with 13 turbines to be built and installed, based on the background experience developed during onshore and offshore tests. The *Deepwind* project [17, 18, 19] proposed an equivalent floating offshore wind turbine concept, which consists of a long axis that rotates in the water, with a vertical axis Troposkien rotor placed on the top, a generator located at the bottom of the rotor and a sea-bed support structure system [20]. In this system, the vertical axis rotor is targeted to reach a power production of 5 MW. The rotor swept area needed to obtain such power production leads the project researchers to adopt a modified Troposkien shape rotor [21] with a characteristic length of about 130 m.

The aerodynamic performance for these type of rotors was estimated by considering the wind turbine as perfectly vertical (i.e., orthogonal) to the free-stream wind speed, despite the rotor, due to the floating support structure, will mostly operate in a tilted configuration. This approximation is usually made in most conventional semi-empirical models used to simulate the aerodynamic performance of vertical axis wind turbines e.g., the Blade-Element Momentum theory [22, 23, 24] or Vortex models [25]. Tilted conditions are generally treated by reducing the performance of a tilted rotor by considering only the projection of the free-stream wind speed on the rotor plane [26, 27].

The purpose of the present work is to provide a modeling approach to forecast the aerodynamic performance of a tilted Darrieus rotor with a Troposkien shape. The limitations of conventional semi-empirical methods are overcome by considering an unsteady three-dimensional URANS $k-\omega$ SST CFD model, whose validation against experimental data for a 2 meter rotor [2] is presented in this paper. This size is adopted, beside for the availability of experimental data, to compare the numerical predictions with the 2-meter Deepwind demonstrator [28], which is operating in these particular conditions. Results, however, have general validity, since the Troposkien shape is simply scaled for turbines characterized by larger dimensions.

2. Experimental Data

The experimental data provided by Sheldahl [2] of a 2-meter wind turbine are considered in the validation of the URANS-based simulations. The rotor is 2-meter high with a maximum radius of 0.98 m. The blade shape is straight-circular-straight (SCS): this is considered a good approximation of the Troposkien architecture [21] but it is cheaper to manufacture. The physical characteristics of the wind turbine are reported in Table 1, while a picture of the wind turbine installation at the Sandia test site is shown in Figure 1.

H [m]	2
R [m]	0.98
N_B [-]	3
Blade profile	NACA 0012
Blade shape	Straight-circular-straight (SCS)
c [mm]	58.77

Table 1. Main geometrical features of the baseline rotor configuration.

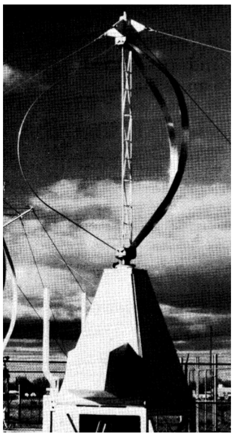

Figure 1. Sandia 2-meter Darrieus wind turbine installation (from: [2]).

Open-field and wind tunnel tests were conducted considering two rotational speeds, 400 *rpm* and 460 *rpm*. The two tests provide results in good agreement with respect to the tip speed ratio. The comparison with the URANS-based simulations is therefore performed considering only the experimental data from the wind tunnel test at a rotational speed of 400 rpm. The technical report [29] indicates that the chord Reynolds number, defined as:

$$Re_c = \frac{\omega R c}{\nu} \tag{1}$$

was kept constant for this specific test at a value of $1.54 \cdot 10^5$.

The cinematic viscosity for the test can be evaluated and results to be $\nu = 1.566 \cdot 10^{-5}\ m^2/s$. This value is different from the common reference value at the standard sea level, which will be also adopted in the CFD simulation. In fact, considering an air density of $\rho = 1.225\ kg/m^3$ and a dynamic viscosity of $\mu = 1.789 \cdot 10^{-5}\ kg\ m/s$ [30], the cinematic viscosity at the standard sea level is $\nu = 1.460 \cdot 10^{-5}\ m^2/s$.

Retaining the original chord Reynolds number, a corrected rotational speed can be calculated from the standard cinematic viscosity, which results to be 371.09 rpm. The tip speed ratios are also corrected and a shifted performance curve is obtained, which is reported in Figure 2. This curve, which represents the rotor efficiency at the standard sea level, is considered in the following CFD validation.

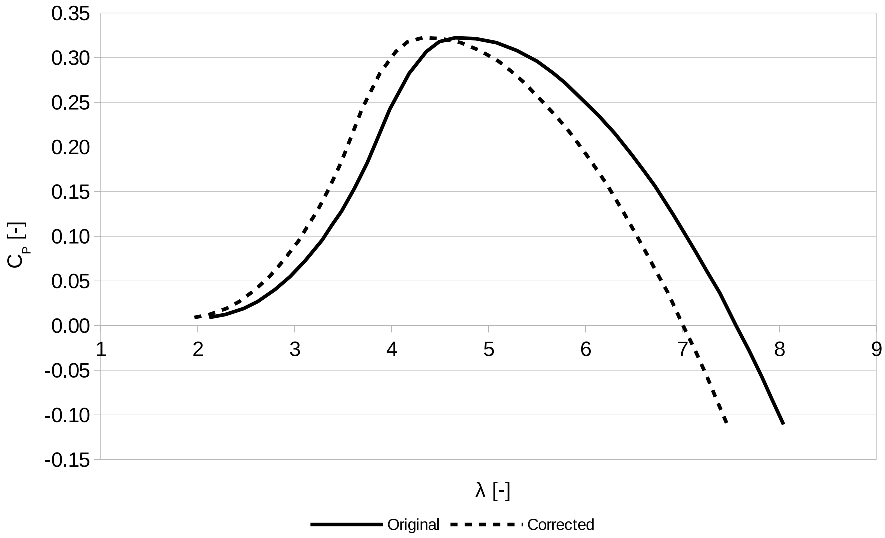

Figure 2. Original and cinematic viscosity corrected performance of the Sandia 2-meter rotor from the wind tunnel test.

3. CFD Validation

The URANS CFD simulations are conducted employing the commercial software Ansys Fluent 14.5 [31]. The adopted turbulence model is the $k - \omega$ SST. This model was chosen due to its accuracy and reliability to predict complex aerodynamics under a wide of fluid flow conditions, including cases with adverse pressure gradients acting on two-dimensional airfoils [32, 33]. The introduction of a blending function, which combines the Wilcox $k - \omega$ model and the standard $k-\epsilon$, ensures that the model equations behave appropriately in both the near-wall and far-field zones. In the near-wall boundary, the k equation of the $k-\omega$ SST model is treated in the same way as the k equation of the $k-\epsilon$, which relies on the enhanced wall treatment approach. This means that for spatial discretizations concentrated towards the wall, which are defined by values of the dimensionless wall distance y^+ [31] close or lower than the unity (hereinafter referred as "fine meshes"), the appropriate low-Reynolds-number boundary condition is applied, while the wall function approach is used for meshes characterized by y^+ values larger than unity, hence properly taking into consideration the inner layers of the boundary layer. [31]. The simulation is set to unsteady with a timestep equal to the time needed for the rotor to perform an azimuthal rotation of 1 degree. The spatial and temporal discretizations are performed considering second order schemes. The time-step converges when the scaled residual values [34] fell below 10^{-5}, since lower values would not lead to sensible difference in the estimations [35]. The rotor torque varies in every time step due to the simulation unsteadiness. The final average torque value T is estimated when the simulation is considered as periodic, i.e. when the difference between average torque values in sequential rotational periods is lower than 1%. This value is adopted to compute the power production P and the power coefficient C_P, in formulas:

$$C_P = \frac{P}{0.5 \cdot \rho \cdot A \cdot v^3} = \frac{T \cdot \omega}{0.5 \cdot \rho \cdot A \cdot v^3} \tag{2}$$

The Sandia turbine is modelled as a three-blade rotor with the physical characteristics reported in Table 1. The three blades are connected with each other on the top and the bottom of the rotor through the introduction of two truncated cones. The central shaft is disregarded in the simulation due to the lack of information about its geometry [2], and due to the limited effect of its wake, which affects only the downwind production [32, 35, 36]. This approximation moreover helps to reduce the computational complexity.

The simulation domain is rectangular with an allowance axial and vertical distances respectively of 20 *m* and 3 *m*. This shape is selected to reproduce a virtual wind tunnel with neglectable blockage effects: the adopted distances, largely greater than 10 times the chord length, were chosen to minimize the influence of the boundary walls. The domain is divided into two sub-domains, *gallery* and *cylinder*, to define different spatial discretizations and the rotor motion in the *cylinder* domain. The two domains are shown in Figure 3, where the size and the boundary conditions are also indicated. The validation case with the 2-meter rotor presents a perfect symmetry between the top and the bottom rotor halves, since a uniform wind speed is imposed at the velocity-inlet. Thus only half of the rotor is simulated, placing a symmetry boundary condition at the rotor middle plane. A *velocity inlet* boundary is imposed at the inlet, considering a uniform wind speed. The outlet is considered as a *pressure outlet*, with a gauge pressure of 0 *Pa*. Since the simulation aims to reproduce the wind tunnel tests, a low level of turbulence is set both at the inlet and the outlet: the turbulence intensity was 0.1% and the turbulent viscosity ratio was 10, as suggested by the software

User Guide [37]. The blades are considered as *no-slip walls*. Since additional details are not provided by the reference paper from Sheldahl [2], walls are considered smooth with a roughness height of 0 *m*.

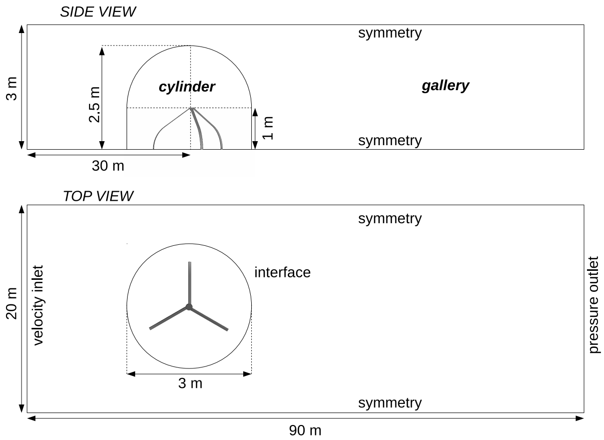

Figure 3. Scheme of the computational domains with boundary conditions and sizes.

A sensitivity analysis is conducted to study the most important mesh parameters. A hexahedral mesh extrusion is created over the rotor blades, in order to simulate the blade's boundary layer. The first element height is estimated by imposing the maximum y^+ value in all the rotor near-wall cells to be lower than 1, an approximated value which is reported to maximize the reliability of the turbulence model [31]. The number of mesh extrusion steps and the growth rate were object of investigation, since these parameters strongly influence the total number of discretized elements, while other parameters are kept constant as reported in Table 2.

Number of elements on the blade airfoil	244
Number of elements on the blade lenght	300
Leading edge spacing [mm]	0.15
Trailing edge spacing [mm]	0.20
First layer height [mm]	0.011
Cylinder wall mean element size [mm]	85
Gallery wall mean element size [mm]	350
Volume mesh growth rate	1.15

Table 2. Geometrical parameters of the baseline mesh.

Two different configurations for the boundary layer extrusions were considered:

(i) 27 steps with a growth rate of 1.15;

(ii) 15 steps, 10 layers with a growth rate of 1.15 and 5 layers with a growth rate of 1.5.

Simulations are conducted considering tip speed ratios between 2 and 6 and the results are reported in Figure 4. The peak power coefficients and their tip speed ratios obtained with both mesh configurations are close to the experimental data. A good agreement is also registered with both mesh configurations at high tip speed ratios, whereas for low tip speed ratios the mesh with 15 steps is overpredicting the performance. The difference is, however, very limited.

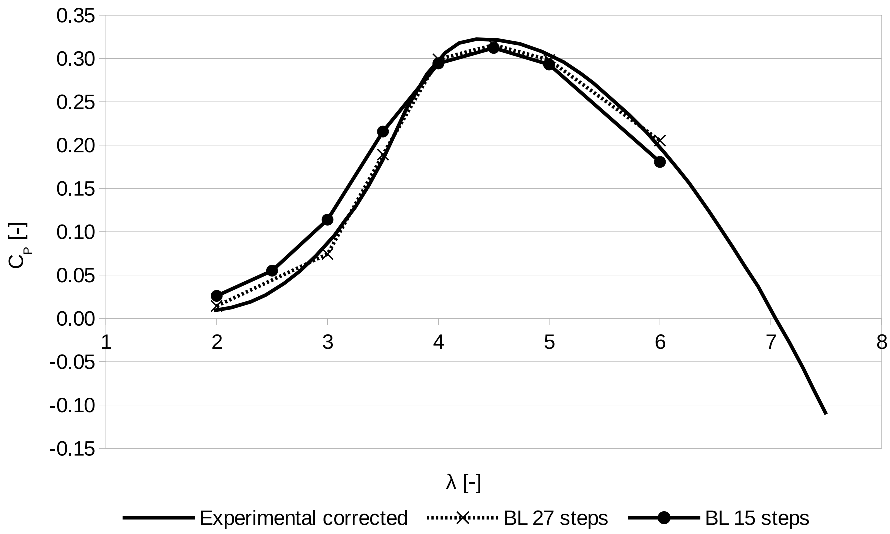

Figure 4. Simulation results with two different configurations for the boundary layer extrusion.

Moreover, the mesh with 15 steps is capable to capture completely the boundary layer when the airfoil is not stalling. The turbulent viscosity ratio experiences, in fact, a large rise and dissipation confined in the prism layer, as can be seen in Figures 5(a) and 5(b) for two azimuthal positions. This is not observed in Figure 5(c) for a different azimuthal position, since the airfoil stalls and the boundary layer is detached.

On the other hand, the simulation of a tilted Darrieus turbine requires two times the number of discretized elements, since the the blade airfoils from the upper and lower rotor halves would interact with the fluid at different angles of attack. The number of elements required for the configuration with 27 step extrusion is not compatible with the available computational power, since it exceeds the 64 GB RAM requirements. Therefore the configuration with 15 step extrusion is selected, showed in Figure 6.

A sensitivity analysis is also conducted with respect to the number of elements on the base airfoils of the blade on a single operative condition, $\lambda = 4$. The simulation results are reported in Table 3. The CFD simulation with the higher number of elements is closer to the experimental result. On the other hand, a small difference is registered in the power coefficient values estimated by CFD simulations and, due to the limitation in the RAM usage, the configuration with 244 elements on the profile is adopted.

The mesh is characterized by 13.8 millions of cells and the unsteady simulation requires about 60 GB of RAM memory. A computer equipped with a 8-core Intel Xeon E5-2650 2.00 Ghz takes about 10 minutes to complete a

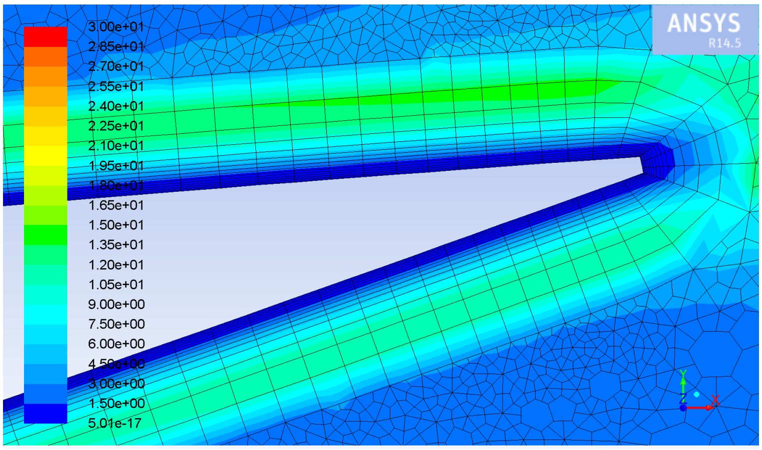

(a) β = 12°

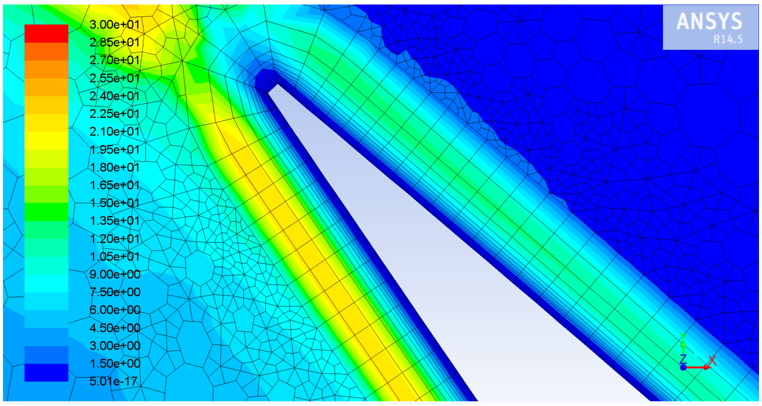

(b) β = 132°

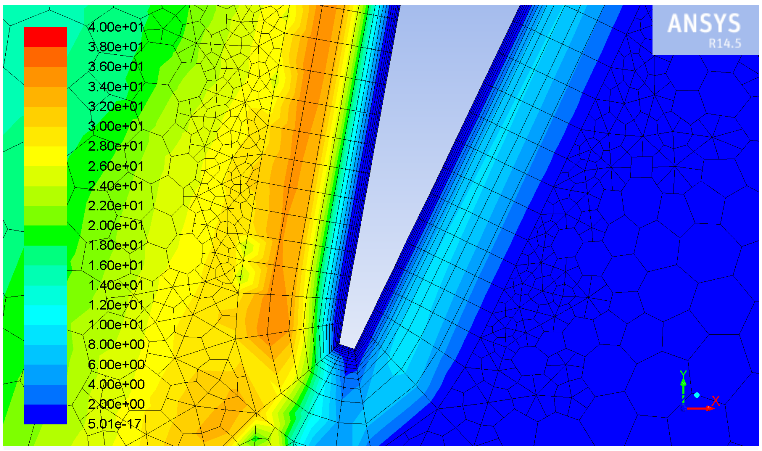

(c) β = 252°

Figure 5. Turbulent viscosity ratio near the airfoil at different azimuthal positions, λ = 4.5.

single time-step, whereas the final torque value is obtained after the simulation of 2500 time-steps on average.

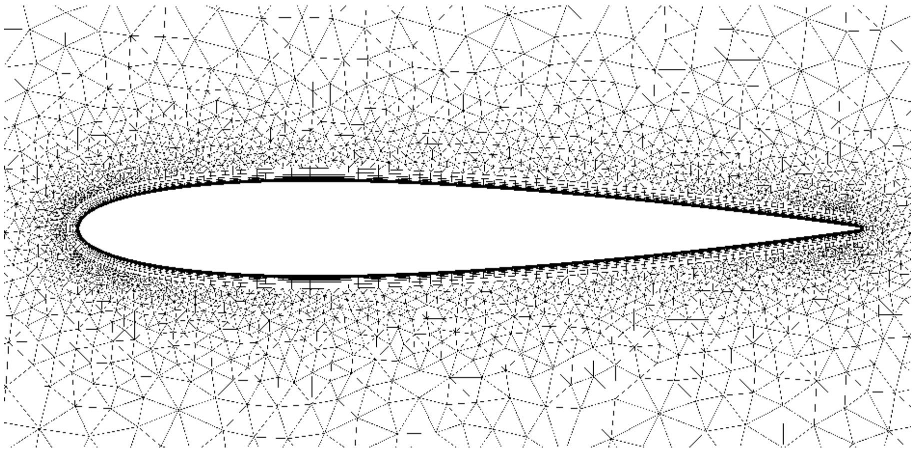

Figure 6. Airfoil mesh with 15 step boundary layer extrusion.

Configuration	Power Coefficient [-]
Experimental corrected	0.300
CFD, 244 elements on profile	0.294
CFD, 364 elements on profile	0.304

Table 3. Simulation results for λ = 4 with two number of elements on the profile of the blade airfoil.

4. Results and Discussion

The domain for the tilted Darrieus simulation is created by rotating the *cylinder* domain around the rotor virtual central point with a defined angle. The *gallery* domain is reconstructed afterwards, as showed in Figure 7. The rotor rotation and the torque calculation are specified considering the new tilted axis.

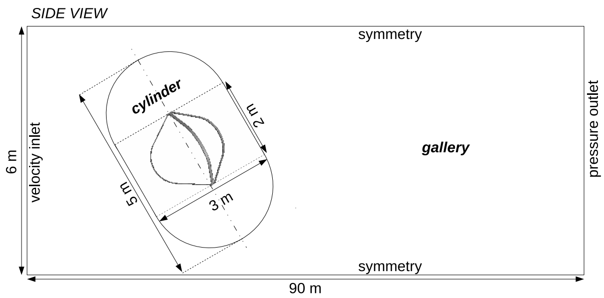

Figure 7. Scheme of the computational domains for the tilted configuration with boundary conditions and sizes, no to scale.

During offshore operations, the rotor blades should not impact the water during rotation. The tilt angle is therefore expected, and should be forced, not to exceed the angle at the Troposkien root, which is about 30°. Simulations are therefore conducted considering two tilted configurations, with a tilt angle equals to 10° and 20°. The power production P with respect to the free-stream wind speed v and the power coefficient C_P with respect to the tip speed ratio λ for the two tilted configurations are reported in Figure 8, whereas the peak power coefficient values, the relative tip speed ratios and their variations with respect to the vertical configuration are reported in Table 4.

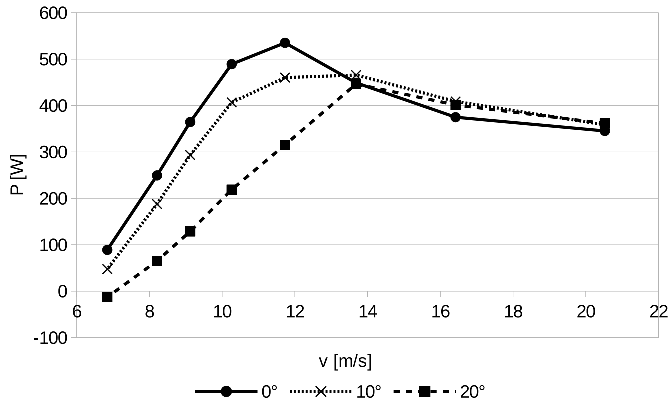

(a) Power production with respect to the wind speed.

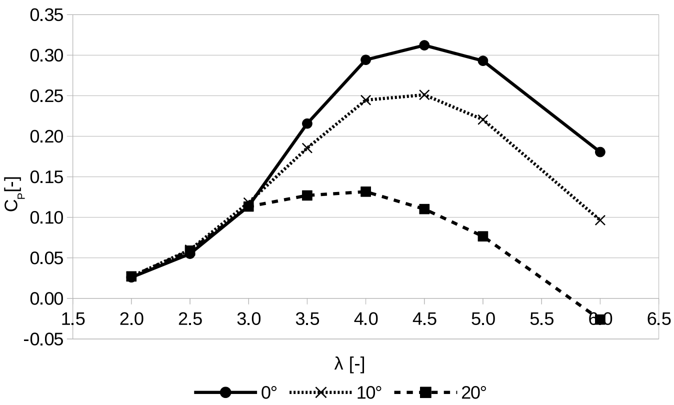

(b) Power coefficient with respect to the tip speed ratio.

Figure 8. Aerodynamic performance for the two tilted configurations obtained with the URANS CFD simulations.

Configuration	$\lambda\vert_{\max C_P}$ [-]	$\max C_P$ [-]	$\Delta\lambda\vert_{\max C_P}$ [-]	ΔC_P [-]
0°	4.5	0.3122		
10°	4.5	0.2511	0.00%	-19.57%
20°	4.0	0.1316	-11.11%	-57.83%

Table 4. Peak power coefficient values, relative tip speed ratios and variations with respect to the vertical configuration.

The comparison between the performance of the non-tilted and tilted rotors can be analysed by considering the rotor behaviour before and after a particular operative point characterized by the operative condition of $\lambda = 3$, approximately equal to $v = 14 m/s$. The tilted rotor operating at high tip speed ratios, corresponding to lower wind speeds, i.e. lower angles of attack, is experiencing an expected decrease in the power production due to the unfavorable effective wind direction. As reported by Johnson [38], the aerodynamic forces in a yawed wing can be estimated, for small angles of attack, by considering the two-dimensional aerodynamic coefficients but with different wind speeds:

the lift and the drag force should be computed, respectively, using the projected and the free-stream wind speeds, the former lower than the latter. Consequently, the reduction in the lift force with respect to the drag force will lead to a reduction in the rotor torque.

As stated before, this trend is generally considered in the semi-empirical analysis by reducing the inflow wind speed, approximately by the cosine of the tilt angle [26, 27]. Figure 9 shows a comparison between the performance estimated by the URANS CFD approach and those obtained by interpolating the simulation results with a reduced inflow wind speed calculated as:

$$v = v_\infty \cdot \cos\theta \tag{3}$$

The accuracy of the prediction obtained by projecting the wind speed is very limited since performance are over-predicted with respect to the URANS CFD simulations for the lower wind speeds. Whereas a shifting trend of the production curve can be still observed, as the peak production is reduced and moved to higher wind speeds, a more accurate model to be adopted in semi-empirical methods is needed to predict this aerodynamic effect in the tilted rotors.

The tilted rotor performance at tip speed ratios higher than $\lambda = 3$ are instead comparable to the vertical rotor configuration. The power coefficient values are super-imposed whereas a small increase in the power performance is observed. The reason behind this behaviour can be found in the profile aerodynamics. In the operative conditions above the peak power production, in fact, the rotor is operating at stalled conditions with large angles of attack. In these conditions, small variations in the angle of attack, due to the rotor tilt, lead to limited variations around the zero value of the tangential force coefficient C_t [22], defined as:

$$C_t = C_L \sin\alpha - C_D \cos\alpha \tag{4}$$

The coefficient values with respect to different angles of attack derived from the experimental NACA 0012 coefficient database developed by Jacobs [39] and extended by Bedon et al. [11] are plotted in Figure 10 for two Reynolds numbers typical of these operative conditions. Variations in the rotor torque, calculated from the average C_t value, are therefore limited too. This explanation can be also confirmed by observing that the performance obtained by projecting the wind speed on the rotor plane, which involves a small change in the angle of attack, are in good agreement with those from URANS CFD simulations. Moreover, since the three-dimensional nature of the separated flow due to the boundary layer detachment influences the whole blade aerodynamics [40], no relevant differences between the tilted and vertical configurations should be expected.

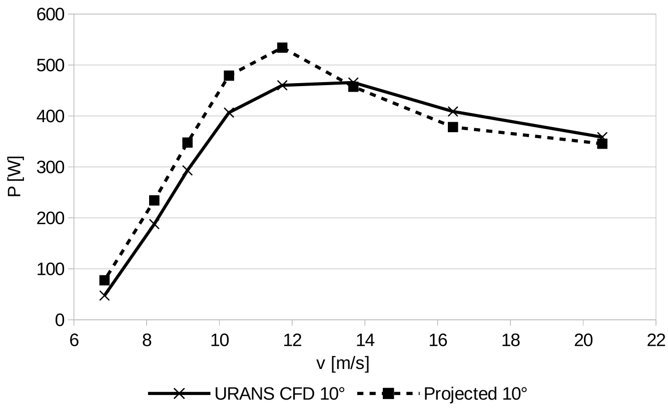

(a) Tilt angle of 10°.

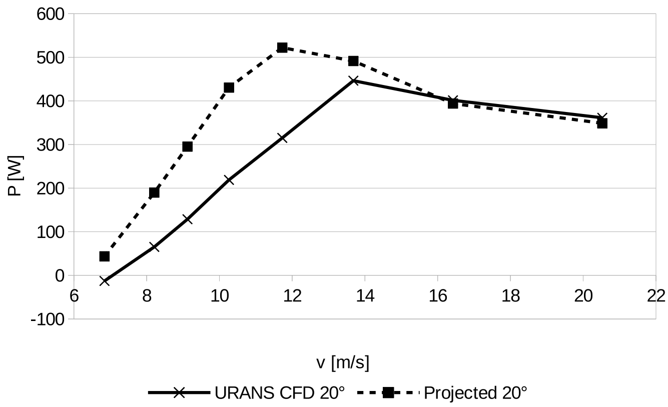

(b) Tilt angle of 20°.

Figure 9. Performance of the two tilted configurations, estimated by URANS CFD simulations and interpolation of the curve with a reduced wind speed.

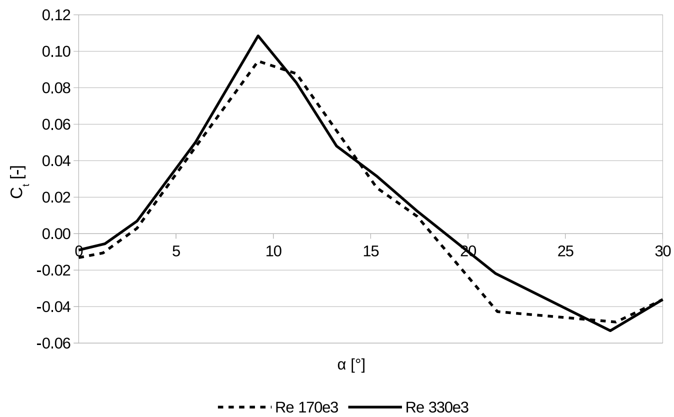

Figure 10. Tangential force coefficient C_t with respect to the angle of attack for two operational Reynolds numbers.

5. Conclusions and Future Works

This work presented a CFD-based study of the aerodynamic performance of a Darrieus wind turbine operating under tilted conditions.

As a first step, an URANS approach based on the $k-\omega$ SST turbulence model was developed to predict the unsteady aerodynamics of the Darrieus rotor. A sensitivity analysis was conducted to determine the proper value of the most important parameters of the finite-volume domain discretization. Acceptable agreement between the experimental and the numerical results in non-tilted conditions was found, enabling the use of the model for the analysis of the tilted configurations.

Two tilt angles were considered due to the operative restrictions linked to the Troposkien shape: 10° and 20°. The performance of the vertical-axis wind turbine was reported in terms of the power production and the power coefficient. As expected, a reduced performance was observed with increasing tilt angle. However, two different trends were observed as a function of the tip speed ratio. For high tip speed ratios, a strong decrease in the power coefficient was observed. This performance attenuation is linked to the yawed airfoil theory. A comparison between the URANS estimations and the results obtained by simply projecting the wind speed along the rotor plane highlighted the limitation of the second approach, which is unable to account for the three-dimensional effects due to the tilted inflow. At low tip speed ratios, the tilted rotor performance was comparable with the perfectly vertical configuration. This behaviour is linked to the stalled operative conditions of the rotor, since the tangential coefficient C_t is little varying with a variation of the angle of attack. Estimations based on the wind speed projection, which relies on the same hypothesis, are in fact accurate.

These computational predictions represent the first attempt to provide an estimation of the aerodynamic performance in tilted configurations, which are often experienced in offshore conditions. A validation with experimental results would provide a final confirmation on the accuracy of the CFD approach and would allow to perform a deeper analysis of the Darrieus aerodynamics in these unconventional operative conditions. Moreover, corrections for semi-empirical models could be developed in order to overcome the actual limitations, leading to more complete theories which could be adopted in much comprehensive analyses.

Nomenclature

A $[m^2]$	Rotor swept area
c $[m]$	Airfoil chord
C_D $[-]$	Airfoil drag coefficient
C_L $[-]$	Airfoil lift coefficient
C_P $[-]$	Rotor power coefficient
C_t $[-]$	Tangential force coefficients
H $[m]$	Rotor height
N_B $[-]$	Number of blades
P $[W]$	Power produced by the turbine
R $[m]$	Rotor maximum radius
Re_c $[-]$	Chord Reynolds number
T $[Nm]$	Final average torque value
v $[m/s]$	Reference wind velocity
v_∞ $[m/s]$	Free-stream wind velocity
y^+ $[-]$	Dimensionless wall distance
α $[°]$	Airfoil angle of attack
β $[°]$	Airfoil azimuthal position
λ $[-]$	Tip speed ratio
μ $[kg\ m/s]$	Dynamic viscosity
ν $[m^2/s]$	Cinematic viscosity
ρ $[kg/m^3]$	Air density
θ $[°]$	Rotor tilt angle
ω $[rad/s]$	Rotor rotational speed

References

[1] American Wind Energy Association, U.S. Wind Industry Annual Market Report 2014, Tech. rep., American Wind Energy Association, Washington, D.C., U.S.A. (2014).

[2] R. E. Sheldahl, Comparison of field and wind tunnel Darrieus wind turbine data, Tech. rep., Sandia National Laboratories Report SAND80-2469 (1981).
URL http://infoserve.sandia.gov/sand_doc/1980/802469.pdf

[3] R. E. Sheldahl, P. C. Klimas, L. V. Feltz, Aerodynamic performance of a 5-metre-diameter Darrieus turbine with extruded aluminum NACA-0015 blades, Tech. rep., Sandia National Laboratories Report SAND80-0179 (1980).
URL http://www.wrapwind.com/download/800179.pdf

[4] M. H. Worstell, Aerodynamic performance of the 17-metre-diameter Darrieus wind turbine, Tech. rep., Sandia National Laboratories Report SAND78-1737 (1979).
URL http://prod.sandia.gov/techlib/access-control.cgi/1978/781737.pdf http://www.estonia.ca/koit/Kool/L?put??/Muud materjalid/Sandia/Teisej?rgulised/Sandia 781737.pdf

[5] M. H. Worstell, Aerodynamic performance of the 17-m-diameter Darrieus wind turbine in the three-bladed configuration: An addendum, Tech. rep., Sandia National Laboratories Report SAND79-175 (1982).
URL http://adsabs.harvard.edu/abs/1980STIN...8026857W

[6] T. D. Ashwill, Measured data for the Sandia 34-meter vertical axis wind turbine, Tech. rep., Sandia National Laboratories Report SAND91-2228 (1992).
URL http://infoserve.sandia.gov/sand_doc/1991/912228.pdf

[7] R. J. Templin, R. S. Rangi, Vertical-axis wind turbine development in Canada, IEE Proceedings A Physical Science, Measurement and Instrumentation, Management and Education, Reviews 130 (9) (1983) 555. doi:10.1049/ip-a-1.1983.0085.
URL http://digital-library.theiet.org/content/journals/10.1049/ip-a-1.1983.0085

[8] R. D. McConnell, J. H. Vansant, M. Fortin, B. Piché, An experimental 200 kW vertical axis wind turbine for the Magdalen Islands, in: 11th Intersociety Energy Conversion Engineering Conference, American Institute of Chemical Engineers, New York, 1976, pp. 1798–1802.
URL http://adsabs.harvard.edu/abs/1976iece.conf.1798M

[9] J. Déry, Éole, aérogénérateur à axe vertical de 4 MW à Capchat, Québec, Canada, in: Intersol Eighty Five: Proceedings of the Ninth Biennial Congress of the International Solar Energy Society, 1986, pp. 2030–2034.

[10] H. Benjannetm, Structural Design for 4 MW VAWTG - Project Eole, in: Intersol Eighty Five: Proceedings of the Ninth Biennial Congress of the International Solar Energy Society, 1986, pp. 2047–2051.

[11] G. Bedon, E. G. A. Antonini, S. De Betta, M. Raciti Castelli, E. Benini, Evaluation of the Different Aerodynamic Databases for Vertical Axis Wind Turbine Simulations, Renewable & Sustainable Energy Reviews 40 (2014) 386–399.

[12] C. N. Elkinton, Offshore Wind Farm Layout Optimization, Ph.D. thesis, University of Massachusetts (2007).
URL http://books.google.com/books?id=oJ8qKheYDQkC&pgis=1

[13] P. Gardner, A. Garrad, P. Jamieson, H. Snodin, G. Nicholls, A. Tindal, Volume 1: Technology., in: Wind Energy - The Facts, European Wind Energy Association, Brussels, Belgium, 2004.

[14] H. Svensson, Design of foundations for wind turbines, M.Sc. Thesis - Lund University.

[15] M. Raciti Castelli, S. De Betta, E. Benini, Preliminary Evaluation of Feasibility for Wind Energy Production on Offshore Extraction Platforms, Wold Academy of Science, Engineering and Technology 6 (11) (2012) 1873–1878.

[16] http://www.inflow-fp7.eu/, accessed on February 2015.

[17] L. Vita, Offshore Floating Vertical Axis Wind Turbines with Rotating Platform, Risø-phd-80(en), Danmarks Tekniske Universitet (2011).

[18] U. Schmidt Paulsen, L. Vita, H. Aagård Madsen, J. H. Hattel, E. Ritchie, K. M. Leban, P. A. Berthelsen, S. Carstensen, 1st DeepWind 5 MW baseline design, Energy Procedia 24 (2012) 27–35.

[19] U. Schmidt Paulsen, H. Aagård Madsen, J. H. Hattel, I. Baran, P. Hørlyck Nielsen, Design Optimization of a 5 MW Floating Offshore Vertical-axis Wind Turbine, Energy Procedia 35 (2013) 22–32.
URL http://www.sciencedirect.com/science/article/pii/S1876610213012411

[20] http://www.deepwind.eu/The-DeepWind-Project, accessed on February 2015.

[21] G. E. Reis, B. F. Blackwell, Practical approximations to a troposkien by straight-line and circular-arc segments, Tech. rep., Sandia National Laboratories Report SAND74-0100 (1975).
URL http://www.osti.gov/energycitations/product.biblio.jsp?osti_id=5115217

[22] J. H. Strickland, The Darrieus Turbine: A performance prediction model using multiple streamtubes, Tech. rep., Sandia National Laboratories Report SAND75-0431 (1975).
URL http://scholar.google.com/scholar?hl=en&btnG=Search&q=intitle:The+Darrieus+Turbine:+A+performance+prediction+model+us

[23] I. Paraschivoiu, Double-multiple streamtube model for Darrieus in turbines, in: Wind Turbine Dynamics, Nasa Conference Publication 2185, Cleveland, Ohio, USA, 1981, pp. 19–25.
URL http://onlinelibrary.wiley.com/doi/10.1002/cbdv.200490137/abstract http://adsabs.harvard.edu/abs/1981wtd..nasa...19P

[24] I. Paraschivoiu, F. Delclaux, Double multiple streamtube model with recent improvements, Journal of Energy 7 (3) (1983) 250–255.
URL http://adsabs.harvard.edu/abs/1983JEner...7..250P

[25] J. H. Strickland, B. T. Webster, T. Nguyen, A Vortex Model of the Darrieus Turbine: An Analytical and Experimental Study, Journal of Fluids Engineering 101 (4).
URL http://www.csa.com/partners/viewrecord.php?requester=gs&collection=TRD&recid=A8018620AH

[26] A. Bianchini, G. Ferrara, L. Ferrari, S. Magnani, An Improved Model for the Performance Estimation of an H-Darrieus Wind Turbine in Skewed Flow ACRONYMS, Wind Energy 36 (6) (2012) 667–686. doi:10.1260/0309-524X.36.6.667.

[27] K. Wang, M. Otto Laver Hansen, T. Moan, Model improvements for evaluating the effect of tower tilting on the aerodynamics of a vertical axis wind turbine, Wind Energy 18 (January 2015) (2015) 91–110. doi:10.1002/we.
URL http://onlinelibrary.wiley.com/doi/10.1002/we.1608/full

[28] U. Schmidt Paulsen, T. Friis Pedersen, H. Aagård Madsen, K. Enevoldsen, P. Hørlyck Nielsen, J. H. Hattel, L. Zannel, L. Battisti, A. Brighenti, M. Lacaze, V. Lim, J. W. Heinen, P. A. Berthelsen, S. Carstensen, E.-J. De Ridder, G. van Bussel, G. Tescione, Deepwind - An Innovative Wind Turbine Concept for Offshore, in: EWEA 2011 Conference, 2011.
URL http://proceedings.ewea.org/annual2011/allfiles2/1269_EWEA2011presentation.pdf

[29] B. F. Blackwell, R. E. Sheldahl, L. V. Feltz, Wind tunnel performance data for the Darrieus wind turbine with NACA 0012 blades, Tech. rep., Sandia National Laboratories Report SAND76-013 (1976).
URL http://www.osti.gov/energycitations/product.biblio.jsp?osti_id=7269797

[30] B. W. McCormick, Aerodynamics, aeronautics and flight mechanics, 1994.
URL http://as.wiley.com/WileyCDA/WileyTitle/productCd-0471575062.html

[31] Ansys Inc., ANSYS FLUENT 14.5 Theory Guide, Canonsburg, PA, U.S.A., 2012.

[32] M. Raciti Castelli, G. Ardizzon, L. Battisti, E. Benini, G. Pavesi, Modeling Strategy and Numerical Validation for a Darrieus Vertical Axis Micro-Wind Turbine, in: ASME 2010 International Mechanical Engineering Congress & Exposition IMECE2010-39548, Vancouver, British Columbia (Canada), 2010.
URL http://link.aip.org/link/abstract/ASMECP/v2010/i44441/p409/s1

[33] F. Balduzzi, A. Bianchini, R. Maleci, G. Ferrara, L. Ferrari, Blade Design Criteria to Compensate the Flow Curvature Effects in H-Darrieus Wind Turbines, Journal of Turbomachinery 137 (January) (2015) 1–10. doi:10.1115/1.4028245.

[34] Ansys Inc., ANSYS FLUENT 14.5 User's Guide, Canonsburg, PA, U.S.A., 2012.

[35] M. Raciti Castelli, A. Englaro, E. Benini, The Darrieus wind turbine: Proposal for a new performance prediction model based on CFD, Energy 36 (8) (2011) 4919–4934. doi:10.1016/j.energy.2011.05.036.

URL http://linkinghub.elsevier.com/retrieve/pii/S0360544211003616

[36] M. Raciti Castelli, E. Benini, Effect of blade inclination angle on a Darrieus wind turbine, Journal of Turbomachinery 134 (2012) 031016–1–10.
URL http://cat.inist.fr/?aModele=afficheN&cpsidt=25783928

[37] Ansys Inc., ANSYS FLUENT 14.0 Theory Guide, Canonsburg, PA, U.S.A., 2011.
URL http://scholar.google.com/scholar?hl=en&btnG=Search&q=intitle:ANSYS+FLUENT+Theory+Guide#1

[38] W. Johnson, Helicopter theory, Dover Publications, 1980.

[39] E. N. Jacobs, A. Sherman, Airfoil section characteristics as affected by variations of the Reynolds number, Tech. rep., National Advisory Committee for Aeronautics 586 (1937).
URL http://aerade.cranfield.ac.uk/ara/1937/naca-report-586.pdf

[40] J. Katz, Large-Scale Vortex-Lattice Model for the Locally Separated Flow over Wings, American Institute of Aeronautics and Astronautics Journal 20 (12) (1982) 1640–1646.